CALPHAD: Computer Coupling of Phase Diagrams and Thermochemistry 89 (2025) 102821

Contents lists available at ScienceDirect

Calphad

journal homepage: www.elsevier.com/locate/calphad

Thermodynamic assessment of the sulfur and the nickel-sulfur systems

Wenhao Ma [a,*], Julian Gebauer [a], Andreas Klaus Czerny [a], Maryam Rahimi Chegeni [b], Isabella Gallino [b,c], Ralf Busch [b], Hans Jürgen Seifert [a]

[a] Karlsruhe Institute of Technology, Institute for Applied Materials - Applied Materials Physics (IAM-AWP), Hermann-von-Helmholtz-Platz 1, 76344 Eggenstein-Leopoldshafen, Germany
[b] Saarland University, Chair of Metallic Materials, Campus C6.3, 66123 Saarbrücken, Germany
[c] TU-Berlin, Chair of Metallic Materials, Ernst-Reuter-Platz 1, 10587 Berlin, Germany

ARTICLE INFO

Handling Editor: Prof. Z.K. Liu

Keywords:
CALPHAD
Third-generation database
Sulfur
Nickel sulfur system
Supercooled liquid

ABSTRACT

The sulfur and the nickel-sulfur binary systems are important in many fields. In this work, the pure sulfur is remodeled within the framework of the third-generation database approach from 0 K to above the melting point. Likewise, a new thermodynamic dataset is developed for the nickel sulfur binary system. The new thermodynamic dataset provides a reliable description of all relevant intermetallic and non-stoichiometric phases. The supercooled liquid described using the two-state liquid model is considered more realistic. An assessment on the sulfur solubility in FCC nickel is also conducted in this work. The calculated phase diagram, thermodynamic and thermophysical data show good agreement with the literature.

1. Introduction

The unary sulfur and the nickel-sulfur binary system are of significant interest due to their importance in the field of mineralogy [1], metallurgy [2], catalysts [3], superalloys [4], etc. Recent studies also show promising applications of nickel sulfur as material for thermochemical energy storage [5], low temperature sulfur-containing batteries [6,7], or as a bulk metallic glass-forming system [8,9]. Many developments and applications require a deeper understanding of the behavior of the phases both in the sub-room temperature range and in metastable states, e.g. the supercooled liquid state. However, little attention has been paid in this regard by the second-generation thermodynamic database for pure sulfur and for the nickel-sulfur binary system.

For decades, efforts have been made with the CALPHAD (Calculation of Phase Diagrams) method to describe systems with a more physically accurate description. The two-state liquid model was proposed by Ågren et al. [10,11], which gives a more reliable extrapolation for the supercooled liquid than the polynomial functions. The third-generation database approach is proposed to extend the thermodynamic description down to 0 K with the Einstein function [12,13]. These models have been applied to a number of systems, e.g., Cr-Ni [14], Al-C [15], Fe-Mn-Ti [16], etc.

It has become evident that incorporating more physical equations into the description rather than pure mathematical polynomials could give a more reliable description for the stable phases and a better extrapolation into conditions, where experimental data are difficult to obtain. The Ni-S system has been assessed by Sharma and Chang [17], Waldner and Pelton [18,19]. The Ni-S melt has been described by Larrian [20] with the associate model, and by Kongoli [21] with the quasi-chemical model. In the present work, the current assessment of the Ni-S system is extended down to 0 K using the third-generation database approach. The high-temperature heazlewoodite phases are optimized based on more recent experimental findings [22,23] and suggestions [24].

2. Thermodynamic modeling

2.1. Solid phases

The third-generation approach is applied to describe the solid phases, with the Einstein equation describing the harmonic vibrational heat capacities. The reason to use the Einstein function instead of the Debye function is the difficulty in the integration of the Debye expressions into Gibbs energy descriptions that can be used in most commercially available software. However, as is pointed out by Bigdeli et al. [12], the

* Corresponding author.
E-mail address: wenhao.ma@kit.edu (W. Ma).

https://doi.org/10.1016/j.calphad.2025.102821
Received 21 November 2024; Received in revised form 3 March 2025; Accepted 5 March 2025
Available online 16 March 2025

Debye or Einstein function is based on only one parameter, the characteristic temperature, which is in many cases not sufficient to describe the actual vibrational spectrum of solids in the full temperature range, e.g. carbon [12]. To overcome this issue, a multiple Einstein function procedure in the framework of CALPHAD [12] has been proposed. This has been successfully applied to other non-metallic substances such as silicon [25] and GeO_2 [26]. The heat capacity can be expressed as in Equation (1):

$$C_p = \sum_{i=1}^{n} x_i \bullet 3R\left(\frac{\theta_{E_i}}{T}\right)^2 \frac{e^{\frac{\theta_{E_i}}{T}}}{\left(e^{\frac{\theta_{E_i}}{T}}-1\right)^2} + C_p^{mag} + aT + bT^n \quad (1)$$

where the first part of the equation are multiple Einstein functions describing the harmonic vibrational heat capacity. x_i is the weight function for different Einstein equations. In order to meet the Dulong-Petit rule, the sum of x_i should be 1 or close to 1, so that the C_p value of the substance is in the vicinity of 3R at room temperature. R is the gas constant. θ_{E_i} are Einstein temperatures, C_p^{mag} is the magnetic contribution, which can be described by the Inden-Hilert-Jarl model [27] or the Inden-Hilert-Xiong model [28]. The polynomial terms aT and bT^n encircle the electronic contribution, lattice vibration, the discrepancy between c_v and c_p, as well as the anharmonic vibration of the lattice, etc.

The Gibbs energy model for solid phases can be integrated into Equation (2):

$$G_m = E_0 + \sum_{i=1}^{n} x_i\left(\frac{3}{2}R\theta_{E_i} + 3RT\left[1-\exp\left(\frac{-\theta_{E_i}}{T}\right)\right]\right) + G^{mag} - \frac{a}{2}T^2 - \frac{b}{n(n+1)}T^{n+1} \quad (2)$$

where $\boldsymbol{E_0}$ is the cohesive energy at 0 K, which can be estimated by DFT method.

The modeling of the solid solution is traditionally accomplished by applying the Neumann-Kopp rule, which takes the combination of the Gibbs energy description of the end-components. In this process, the conventional term bT should not be used to avoid the non-zero entropy at 0K, as is stated in the hybrid model [15]. For the Ni-S system, the high temperature phases β1, β2 and α-NiS and FCC (Ni) are also modeled similarly to avoid unphysical properties at low temperature. However, due to the comprehensive literature investigation to those phases, the Neumann-Kopp rule is not used.

It should be noted that other approaches have been developed for the description of heat capacity in the lower temperature range, e.g. Gamsjäger and Wiessner [29] have proposed a general expression for the low-temperature heat capacity with one Debye function and 2 E functions. Obaied et al. [30] have proposed a temperature-dependent Debye temperature solution. Although good results can be obtained with those methods, it is difficult to integrate those expressions into Gibbs energy descriptions that can be used in most commercially available CALPHAD software. These approaches are thus not considered in this work.

2.2. Liquid and supercooled liquid

The second-generation thermodynamic model of the supercooled liquid typically consists of polynomial functions extrapolated numerically from the experimental data of the high-temperature melt. This does not provide meaningful values for entropy and heat capacity data of the supercooled liquid [31]. The two-state liquid model is introduced for describing the liquid phase [10,11], where the supercooled liquid phase is considered to be an intermediate state between solid and liquid, and is thus comprised of atoms in both solid-like state and in liquid-like state. This approach depicts a gradual transformation of the atoms from the liquid state to the solid state upon cooling, as well as a gradual loss of translational degrees of freedom [32]. This model has been introduced for a number of systems [14,33,34] and has later been incorporated into the third-generation database approach. The Gibbs energy expression for the two-state liquid model is given in Equation (4) [11]:

$$G_m^L = (1-\chi)G_m^{sol} + \chi G_m^{liq} + RT[\chi\ln(\chi) + (1-\chi)\ln(1-\chi)], \quad (4)$$

where G_m^{sol} is the molar Gibbs energy of solid-like state atoms, G_m^{liq} is the molar Gibbs energy of liquid-like state atoms, χ is the fraction of liquid-like atoms. The model agrees well with the measurements of many pure metals with low melting points [35]. The expression can be further simplified into Equation (5):

$$G_m^L = G_m^{sol} - RTln\left[\left(1+\exp\left(-\Delta G_m^d / RT\right)\right)\right], \quad (5)$$

where ΔG_m^d is the molar Gibbs energy difference between the two states. The G_m^{sol} was originally derived from the Gibbs energy expression of its corresponding crystalline phase. However, in the framework of the third-generation database approach, the liquid - amorphous phase is considered as a single phase, and Einstein equation is applied to describe the G_m^{sol}. This leads to Equation (6):

$$G_m^{L-am} = \frac{3}{2}\theta_E^{L-am} + 3RT\left[1-\exp\left(\frac{-\theta_E^{L-am}}{T}\right)\right] + E_0{}' + a'T^2 - RTln\left[\left(1+\exp\left(-\Delta G_m^d / RT\right)\right) + G^{add}\right] \quad (6)$$

where θ_E^{L-am} is the Einstein temperature of the liquid-amorphous phase, E_0 is the cohesive energy at 0 K, a' is the fitting parameter. As θ_E^{L-am} cannot be obtained experimentally, the relation $\theta_E^{am} \approx 0.7\theta_E^{cryst}$ is proposed [13].

In many cases, it requires extremely large experimental effort to obtain thermophysical and thermodynamic data for the supercooled liquid. The two-state liquid model provides a more reliable extrapolation to lower temperatures. With this approach, the isentropic temperature [36] can be obtained by comparing the entropy of the supercooled liquid and the crystalline phase. Since the entropy of the liquid phase cannot be lower than that of the corresponding crystalline phase, the isentropic temperature is often considered the "ideal" glass transition temperature, above which the liquid state transforms into the glassy state.

2.3. Superheated crystalline state

Improvements are still being made to the third-generation database approach [37–39]. One of the main focuses is on the issue of the superheated solid phases. As is discussed, in order to sufficiently describe the heat capacity of a solid phase, higher-order parameters bT^n are usually applied. However, the exponential increase of the C_p usually leads to an unrealistically high C_p value at high temperature. This corresponds to a substantial drop of the Gibbs energy, which can cause the re-stabilization of solid phases at higher temperatures. It should be noted that for the pure elements with low melting points, e.g., sulfur, the extrapolation of the unary solid phase to beyond its melting point has a significant effect, as the end members are generally directly referred for the description of the solid solution.

Similar to the supercooled liquid, there is an instability temperature (T_{inst}) in the superheated temperature regime. Bigdeli et al. have attempted to calculate the T_{inst} of aluminum using the DFT method, but the authors claim that the approach needs further improvement [40]. Other attempts have also been made to circumvent this problem. The most frequently used approach is to introduce another segment at superheated temperatures [13]. He et al. [15,37] have proposed a methodology that is capable of describing the solid phase with just one temperature range. The solution is to suspend the solid phase if its entropy is higher than its corresponding liquid phase.

Schmid-Fetzer [39] has later proposed a comprehensive amendment based on the previously mentioned work. The author has suggested that

Table 1
Gibbs energy functions for pure sulfur.

Orthorhombic Sulfur

$${}^{0}G_{S}^{\alpha-S} = -7660.6 - 0.00605*T**2 + 4.227E-36*T**5 + 0.2545*GEIN(196.9) + 0.2283*GEIN(69.01) + 0.3737*GEIN(522.2), 1 < T < 3000$$

Monoclinic Sulfur

$${}^{0}G_{S}^{\beta-S} = G0MONOS + G_{order-disorder} + 0.25*GEIN(180.5) + 0.2005*GEIN(62.42) + 0.3739*GEIN(462.4), 1 < T < 3000$$

Liquid Sulfur

$${}^{0}G_{S}^{Liquid} = -1768.88 - 0.004554**T^2 + G_{LQ2ST} + G_{polymerization} + GEIN(246.08), 1 < T < 3000$$

Functions

$$GEIN(\theta_E) = 1.5*R*\theta_E + 3*R*T*LN\left[1 - \exp\left(\frac{-\theta_E}{T}\right)\right]$$

$$G_{LQ2ST} = -R*T*LN\left(1 + 1*EXP\left(\frac{-5497.36 - 0.05895*T + 0.025945*T*LN(T)}{RT}\right)\right)$$

$$G_{order-disorder} = +0, 1 < T < 180.50;\ 8333.604 - 950.4500*T - 2.2521*T^2 + .00483*T^3 - 5.07922E-06*T**4 + 227.7624*T*N(T), 180.50 < T < 198.50;$$
$$-7183.685 + 107.4215*T - .5339*T^2 + 8.7610E-04*T^3 + 3.1917E-08*T^4 - 79.5378*T^{-1}, 198.50 < T < 200.20;\ 0, 200.20 < T < 6000.00$$

$$G_{polymerization} = 0, 1 < T < 417;$$
$$29241490.4 - 1456638.39*T - 1005.78451*T^2 + .802711556*T^3 - 3.20319381E-04*T^4 + 280050.907*T*LN(T), 417 < T < 434;$$
$$11116027.2 - 219945.77*T - 51.2932*T^2 + .0137829*T^3 + 6.47774447E+08*T^{-1} - 35803.6389*T*LN(T), 417 < T < 470;$$
$$40365.04 + 497.51*T - .0670008*T^2 + 1.19797584E-05*T^3 + -4020722.19*T^{-1} - 74.5463991*T*LN(T), 470 < T < 735;$$
$$1300.7 - 2.64*T, 735\ 0 < T < 6000.00$$

the crystalline phase would collapse into a liquid-like structure at T_{inst}. An additional segment of Gibbs energy description is given at the estimated T_{inst}, which took an estimated value of $1.3 \cdot T_m$. The heat capacity of the superheated solid phase at very high temperature should be equal to the heat capacity of the liquid phase of $2.5 \cdot T_m$. In the example of aluminum, the heat capacity shows a trend, which resembles the two-state liquid model.

On the other hand, not every crystalline phase would show a significant contribution from anharmonic contribution to the heat capacity. In the present work, the multiple Einstein temperature approach can adequately describe e.g. the orthorhombic sulfur phase from 0K to higher temperature with only one segment.

3. Thermodynamic modeling of pure elements

3.1. Nickel

The thermodynamic modeling for nickel is accepted from the work of Hao et al. [41], which is assessed by the third-generation database approach and the modified magnetic model proposed by Xiong et al. [28].

3.2. Orthorhombic sulfur

The physical properties of orthorhombic sulfur (α-S) have been well summarized [42,43]. The comprehensive summary on old publications before 1953 can be found in the Gmelin's handbook [44]. The orthorhombic sulfur is the thermodynamically stable form at room temperature, and has a pale-yellow color. The space group of α-S is Fddd (#70) [45,46]. Early experimental investigations on the heat capacity of the solid-state sulfur have been reported by Regnault [47,48], Nernst [49], Bunsen [50], Mondain-Monval [51], Wigand [52]. The results have been evaluated by Eastman and McGavock [53], where minor deviations (~2 %) are found. More recent evaluations by West [54], Montgomery [55], Mal'tsev and Dmidenko [56], and Hemingway [57] are found consistent with Eastman and McGavock [53].

However, it has been pointed out that many previous measurements of the sulfur can be compromised by unsuspected impurities such as carbon, hydrocarbons, H_2S_x, H_2S, sulfone, sulfoxide, sulfonic and sulfinic acids [58]. The result of c_p measurement by Berezovskii and Paukov [59] deviates slightly from other measurements, which is suspected to be caused by Si impurity. Hemmingway gives a very detailed evaluation on the potential contamination for sulfur from various publications. In this work, the analytical results from Hemmingway with the adiabatic calorimetry is considered the most accurate. The author reports a total impurities of $5 \cdot 10^{-6}$ mass fraction. It is selected for the thermodynamic optimization.

The Debye temperature of sulfur determined by Saunders et al. from ultrasonic-wave velocities is 187.5 ± 2 K [60], while a Debye temperature of 250 K is proposed by Gschneidner [61], which is evaluated from the specific heat data at low temperature. With the relation proposed by Chen and Sundman [62], $\theta_E = 0.714\,\theta_D$, the Gibbs energy description for orthorhombic sulfur can be formulated within the framework of the third-generation database approach. However, both characteristic temperatures cannot describe adequately the heat capacity of orthorhombic sulfur.

It has been mentioned that the orthorhombic sulfur deviates considerably from the Debye behavior [63,64], as the eight-membered ring structure of sulfur would have contributions from the inter- and intra-oscillations. In the work of Bradley, two Debye temperatures, 68 K and 151.5 K, are applied to describe the heat capacity of orthorhombic sulfur with a correction function [63]. However, the resulting C_p^{vib} without correction deviates significantly from the experimental values.

In order to describe the thermophysical properties of sulfur, the multiple Einstein temperature procedure is applied. As is stated by Bigdeli et al., such procedure can be applied to those systems having a strong anisotropy in the lattice [12]. In the present work, 3 E functions (Table 1) are used to describe the orthorhombic sulfur from 0K to higher temperatures with one segment, where satisfactory results are obtained. As is shown in Fig. 1a, b and 1c, the calculated heat capacity and entropy are in good agreement with the experimental [53,55,56] and recommended values [43,55,65]. The calculated standard entropy for orthorhombic sulfur at 298.15K is 31.95 J/mol·K, which is in good aggrement with the literature values: 32.056 ± 0.05 J/mol·K by Chase [43], 31.953 ± 0.083 J/mol·K by Hemingway [57], and 32.070 ± 0.080 J/mol·K by Gurvich et al. [66].

3.3. Monoclinic sulfur

Sulfur transforms from its orthorhombic form to its monoclinic form (β-S) at 368.3 ± 0.3 K with a transition enthalpy of 400.4 ± 3 J/mol, as is obtained by the adiabatic calorimetry measurement of Montgomery [55]. The heat capacity data of monoclinic sulfur have been measured by several groups [53–55], where the results are in good agreement. The space group of monoclinic sulfur is #14: $P2_1/C$ (14) [67]. It shares almost the same ring structure as orthorhombic sulfur, with only small changes in the way of how the rings are packed. Therefore, a description with similar characteristic temperatures as the orthorhombic sulfur is expected.

The monoclinic sulfur is distinguished by an order-disorder transition at 198.3 K [68], which can be observed by a λ-shaped anomaly in

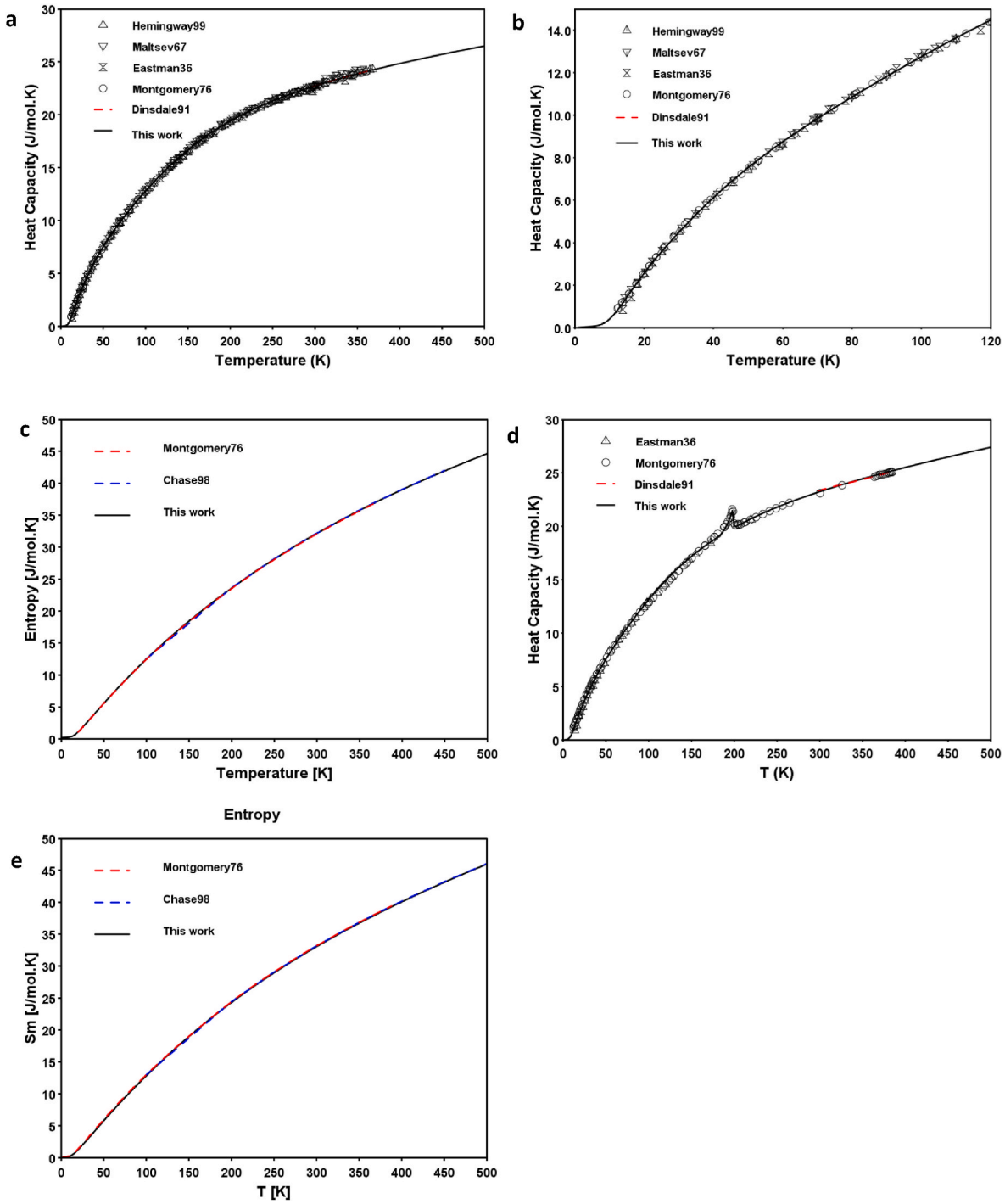

Fig. 1. Comparision between calculated results, experiments and recommended values: a) heat capacity of orthorhombic sulfur; b) heat capacity of orthorhombic sulfur from 0 to 120 K; c) entropy of orthorhombic sulfur; d) heat capacity of monoclinic sulfur; e) entropy of monoclinic sulfur.

the heat capacity measurement. This effect is deconvoluted and expressed separately by a two-segment polynomial function $G_{order-disorder}$, which is later incorporated into the Gibbs energy description of β-S. As shown in Fig. 1d and e, the calculated heat capacity and entropy agree well with the experimental data [53,55] and recommended values [43,55,65], showing the heat capacity value for the order-disorder transition reaching the maximum at 198.3 K.

Both agree well with the value of 360 J/mol recommended by Chase [43]. The calculated phase transition (α-S ⇌ β-S) temperature is 368.3 K, and the calculated enthalpy of transition is 399.9 J/mol, both match well with the results of Montgomery: 368.36 ± 0.3 K and 400.4 ± 2.9 J/mol, respectively [68]. The calculated standard entropy for monoclinic sulfur at 298.15K of is 32.913 J/mol·K, which is in good agreement with the recommended value by Chase: 33.028 ± 0.05 J/mol·K.

In addition to the two stable forms of sulfur, a number of metastable sulfur allotropes have been discovered [69]. These allotropes are not considered in this work.

3.4. Liquid-amorphous sulfur

The melting point of the single crystal β-S is 392.95 K [70]. It should be noted that the melting point of sulfur is usually referred to the natural

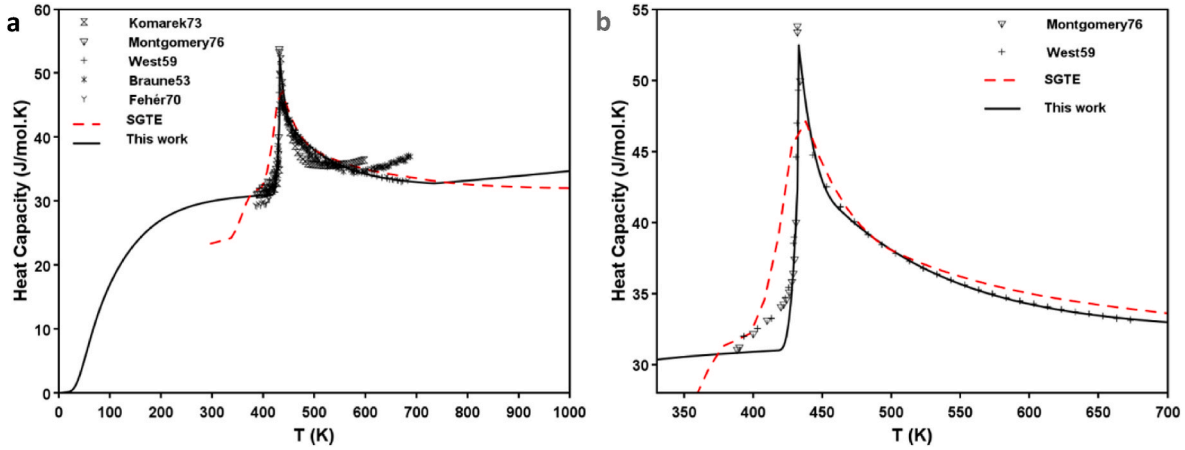

Fig. 2. Comparision between calculated heat capacity and literature data: a) heat capacity of liquid sulfur; b) polymerization peak of liquid sulfur.

melting point, which is the reversible melting point of an equilibrated melt [42]. Montgomery has determined the melting point of sulfur by adiabatic calorimetry measurement to be 388.36 ± 0.02 K, and the enthalpy of fusion to be 1721 ± 8 J/mol [55]. This agrees well with the adiabatic calorimetry measurement conducted by West, where the reported enthalpy of fusion is 1712 ± 10 J/mol at a transition temperature 388.4 ± 0.1 K [54].

Liquid sulfur has a characteristic polymerization behavior, known as the λ transition. The published peak temperature T_λ varies between 432 K and 434.5 K [54,71–75]. It has been reported that the measured polymerization temperature is heavily influenced by the heating rate due to the sluggish kinetics of the reaction [75]. In order to determine T_λ, Kuballa and Schneider have measured the transition temperature at different heating rates; the value of 432.25 K is obtained by extrapolating the measurements to 0 K/min [76]. This result agrees well with the experimental finding of Montgomery et al. at 432.03 ± 0.20 K with a heating rate down to 10^{-5} K/min, [55] and with the result of West at 432.25 ± 0.30 K, which is obtained discontinuously at different temperature segments [54].

The heat capacity of liquid sulfur has been measured by Fehér [74], Komarek [75], Braune [71], West [54], Yoshioka [72], Verryn [77], and Montgomery [55]. The results are similar but show a slight difference depending on the heat rates. The heat capacity data measured by Montgomery [55] are measured under the slowest heat rate, and is therefore used to fit the heat capacity data up to T_λ. At temperatures higher than T_λ, the sluggish polymerization process affects the measured heat capacity substantially, where clear dependence on the heating rate are shown from different groups [75]. In the view of the impact of polymerization on the calorimetric measurement, the heat capacity data for the liquid sulfur above T_λ are taken from the discontinuous heat capacity measurement of West [54]. Similar to the order-disorder transition of β-S, the polymerization is deconvoluted and described by a segmented polynomial function.

Fig. 2 shows the calculated results for experimental data of the liquid sulfur, which are improved from the previous evaluation by the second-generation database. The calculated melting temperature is 388.36 K and the enthalpy of fusion is 1721.1 J/mol. Both are consistent with the experimental findings [54,55]. In addition, the Gibbs energy and entropy extrapolated at temperatures above T_m show reasonable relationship: $G_m^{Liquid} < G_m^{Solid}$; $S_m^{Liquid} > S_m^{Solid}$.

4. Nickel sulfur binary system

4.1. Liquid phase

The Ni-S phase diagram is characterized by a deep eutectic reaction on the Ni-rich side and a liquid miscibility gap on the sulfur-rich side. This is an indication that the liquid phase has a strong short-range order. Therefore, the Ni-S liquid phase is modeled with the associate solution model [78]. Empirically, the hypothetical associate is selected at the concentration corresponding to the stoichiometry of the sulfide with the highest melting point. Therefore, NiS is chosen as the associate for the liquid phase. The liquidus line is plotted based on the experimental data of, Kitakaze [23], Rau [79,80], Kullerud [81], Meyer [82], Nagamori [83], Chuang [84] and Bornemann [85]. As shown in the phase diagram (Fig. 3a), the calculated liquidus line matches excellently with the experimental data. The sulfur activity of the Ni-S melt were measured by Meyer [82], Nagamori and Ingraham [86], Rosenqivst [87], Egami [88], Alcock [89], Takewaki [90], Dashevskiy [91] from 953 K to 1873 K. The calculated sulfur activities at various temperatures are shown in Fig. 3b, where a good agreement can be found with the experimental results.

The supercooled liquid is also described properly by the two-state liquid model [10,11]. Since no experimental data on the supercooled liquid for the Ni-S system can be found, the two-state liquid model with a more physical description is considered to be more reliable than the polynomial description.

It should be noted that it remains unclear whether the polymerization description of the sulfur should be included for the Ni-S liquid phase description, as there is no experimental data on the supercooled nickel sulfur melt. In the new sulfur dataset, the polymerization description can readily be deconvoluted. The model for the liquid phase can therefore be subject to change if there is new experimental insight into the nature of the melt.

4.2. Sulfur solubility in FCC nickel

The modeling of the sulfur solubility in FCC nickel is of scientific and technological importance. It is well known that the introduction of a small amount of sulfur can cause embrittlement of nickel and nickel-based superalloys, especially in the intermediate temperature range from ~500 to 900 °C [92]. Since 1925, studies have been conducted on the mechanism of sulfur-induced embrittlement [93] as well as the solubility of sulfur in FCC-nickel [94]. The sulfur solubility has been studied experimentally by Barbouth and Oudar [95,96], Brigham et al. [94], and Mulford [97]. Their results are consistent with each other.

First-principle calculations have shown that sulfur prefers the substitutional site to the interstitial sites of the FCC Ni [98], which agrees with the assumption of Barbouth [95]. The solubility of sulfur in nickel is thus modeled accordingly. As shown in Fig. 3c, the calculated result is in excellent agreement with the published experimental work. In addition, the vapor pressure of the sulfur in the FCC-Ni has been calculated and compared with measurements of Brigham et a.l [94], and both are close to the Henrian behavior as expected.

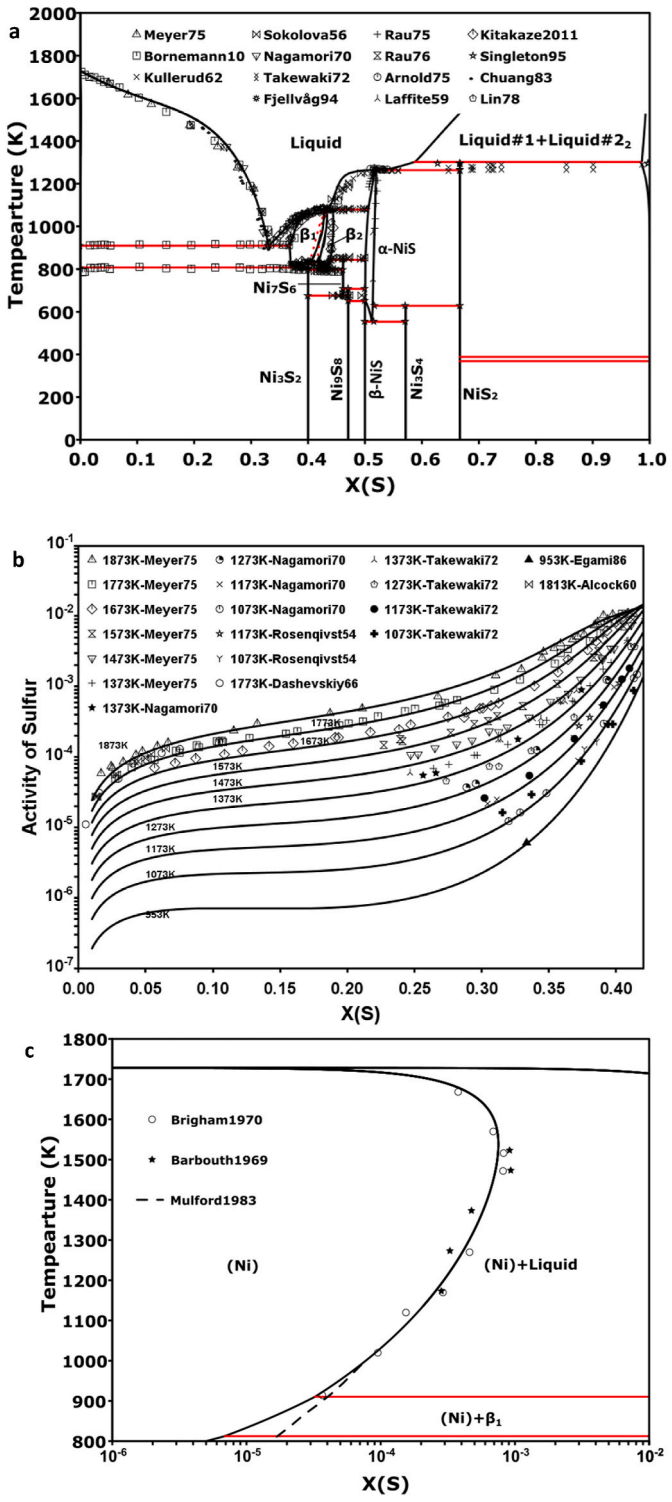

Fig. 3. Calculated results of the Ni-S binary system: a) Ni-S phase diagram; b) sulfur activity of the liquid phase; c) sulfur solubility in the FCC-Ni.

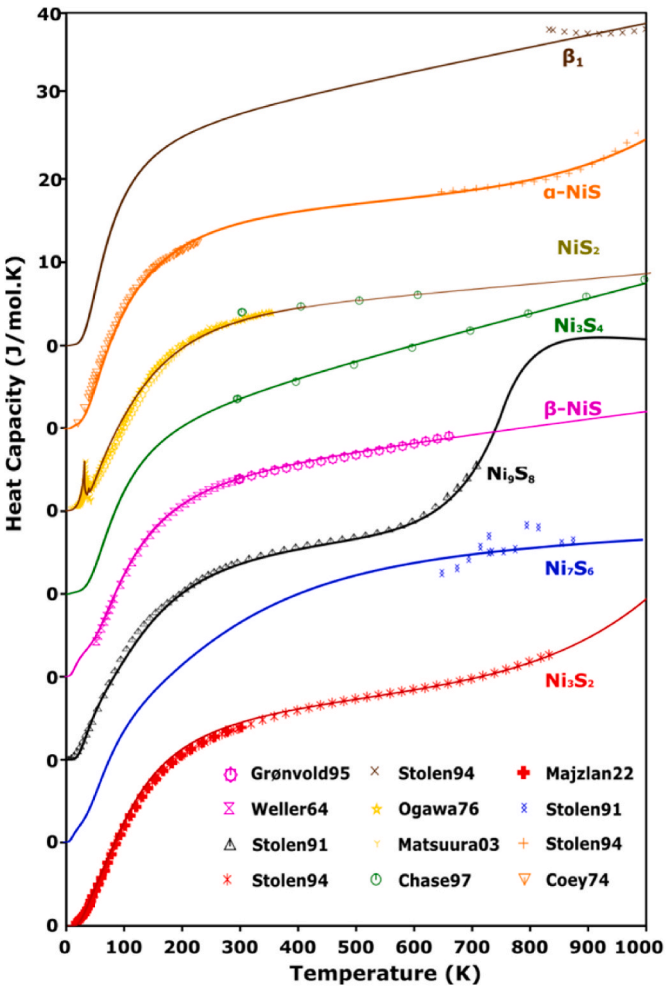

Fig. 4. Comparison between experimental and calculated heat capacities of all nickel sulfides.

4.3. Binary phases

6 stoichiometric compounds are found in the Ni-S binary system: heazlewoodite (Ni_3S_2), millerite (β-NiS), godlevskite (Ni_9S_8), high-temperature godlevskite (Ni_7S_6), polydymite (Ni_3S_4), vaesite (NiS_2).

The space group of Ni_3S_2 is R32 (#155) [99]. The low-temperature heat capacity of Ni_3S_2 was measured by Stølen et al. [100] and Majzlan et al. [101], which agree very well with each other. Ni_3S_2 was considered to transform to its high-temperature form at 834 K, which has a homogeneity range from 36.7 to 42.0 at.%. Later, Rau [80] and Lin et al. [102] found a discontinuity from the activity measurement, and proposed that the high-temperature heazlewoodite, in fact, consists of two phases. However, the EMF measurement conducted by Egami et al. [88], and the XRD measurement by Fjellvåg and Anderson were not able to identify the second phase [103]. Due to the unquenchable nature of the high-temperature heazlewoodite [81], the investigations for the ternary systems including Ni-S through quench experiments did not report the evidence for the β_2 phase [104–106]. The confirmation of the two-phase region is achieved by the high temperature chemical diffusion and electrical conductivity measurements done by Yagi and Wagner [107] and by high-temperature XRD investigation done by Kitakaze and Sugaki [22,23].

Liné and Huber [108] proposed that the space group of β_1 is F $\overline{4}$ 3m (#216), with a lattice parameter of 5.126 Å, which is measured by high temperature XRD measurements. Accordingly, the sulfur atoms are located at Wyckoff positions 4d (0.75,0.75,075); the nickel atoms at the octahedral and tetrahedral voids 4a (0 0 0); 4c (0.25 0.25 0.25). The author proposed that $Ni_{4-\square}S_2$ is the proper notion instead of $Ni_{3\pm x}S_2$, where □ stands for the vacancy. Kitakaze and Sugaki have proposed that β_1 has the space group Fm $\overline{3}$ m (#225) with no detailed information on the crystallography [22]. Stokłosa and Stringer [109] have proposed both vacancies and interstitial sites on both sublattices. However, their conclusion is questioned by Arita [110] because quenched samples were used for the measurement, yet the high-temperature heazlewoodite is

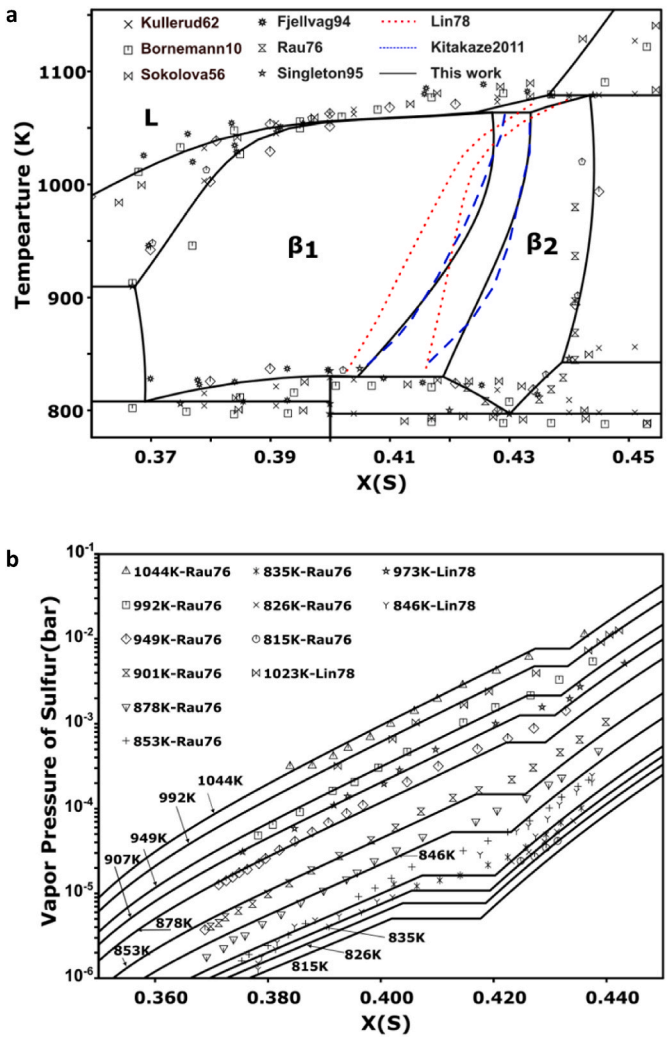

Fig. 5. Comparison between experimental values and calculated results of the Ni-S binary system: a) partial Ni-S phase diagram; b) sulfur vapor pressure of high-temperature heazlewoodites.

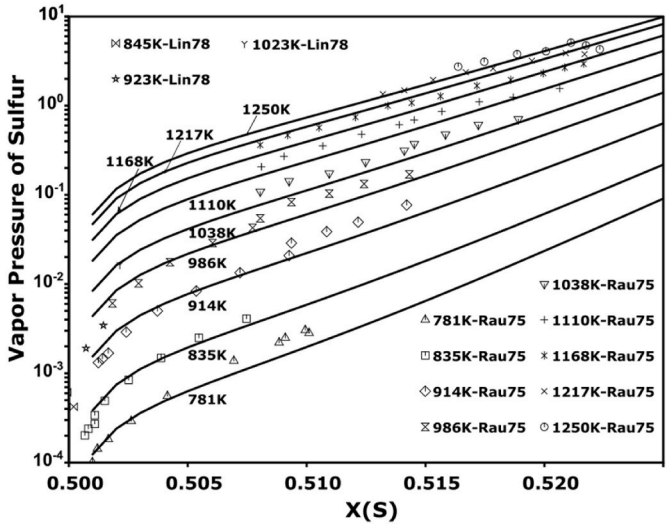

Fig. 6. Comparison between experimental values and calculated sulfur vapor pressure of α-NiS.

not quenchable. Arita [110] has suggested several theoretically possible crystal structures, the calculated vapor pressure based on the assumption are in good agreement with the experimental work of Rau [80], yet no experimental confirmation of the crystalline structure has been reported.

Given the information, the two-sublattice model (Ni, Va)$_2$(S)$_1$ is applied according to Liné and Huber [108]. This is in line with the work of Waldner and Pelton [18]. The crystalline structure of β_2 is reported to be cubic Pn $\overline{3}$ m (#224) [23]. However, the details of the site occupation and crystalline defects are not reported. Considering the similarity in the various experimental data on β_1 and β_2, it is assumed that the two high-temperature heazlewoodite phases have very similar crystalline structure. Therefore, β_2 is modeled with the same two sublattice model as β_1 until further experimental data suggest otherwise. The homogeneity ranges of β_1 and β_2 are taken from the high-temperature XRD measurement by Kitakaze et al. [23]. The heat capacities of heazlewoodites are taken from the evaluation of Stølen et al. from 8 K to 834 K for the low-temperature polymorph, and from 834K to 1000K for β_1 [100]. The experimental heat capacity of β_1 shows a decreasing trend, which can be attributed to the phase transition: $\beta_1 \rightleftharpoons Ni_3S_2$. The comparison between the calculated heat capacity of nickel sulfides and the publications is summarized in Fig. 4.

The phase boundaries between β_1 and β_2 are estimated by Lin et al. [102] from the vapor pressure measurement. The phase boundary cannot be clearly defined due to the similarity of the measured values of the two phases. The high temperature XRD investigation by Kitakaze and Sugaki [22] is carried out at 1 at.% increment, which can provide a qualitative estimation of the phase boundary. A comparison is given at the calculated partial phase diagram (Fig. 5a).

As shown in Fig. 5b, the calculated sulfur vapor pressure of the heazlewoodites (β_1 and β_2) has been carefully compared with the experimental value measured by Rau [80] and Lin et al. [102], where good agreement can be found for temperatures between 815 K and 1044 K. To the best of our knowledge, the heat capacity of β_2 has not been reported. However, it is reasonable to assume that the β_1 and β_2 would have similar heat capacities.

Millerite (β-NiS), with the space group R3m (#160), undergoes a eutectoid reaction and decomposes to α-NiS and Ni_9S_8 at 652 K. The heat capacity data of NiS are taken from the calorimetric study done by Grønvold and Stølen [111]: from 298.15 K to 660 K for β-NiS, and from 660 K to 1000 K for α-NiS. The measured high-temperature heat capacity data of α-NiS start increasing strongly from approximately 850 K. For the metastable α-NiS at low temperature, Coey and Brusetti [112] as well as Trahan and Goodrich [113] have measured from 5 K to 330 K. The results of these two groups agree well with each other, and are both considered for the optimization. The low-temperature heat capacity for β-NiS is obtained from the experimental work of Weller and Kelley from 50 K to 300 K [114]. The heat capacity data measured in this work at around room temperature is compatible with the measurement by Grønvold and Stølen [111].

α-NiS has a NiAs-type crystal structure with the space group P6$_3$/mmc (#186). It is reported to have a homogeneity range from 50 to 51.5 at.% [115]. It is concluded that the sulfur atoms form a hexagonal close packing structure, located at Wyckoff positions 2c (0,0,0); and the Ni atoms occupy the octahedral voids at Wyckoff positions 2a (0,0,0).

A general description has been proposed for the modeling of NiAs-type structure by Jandl et al. [116]. However, given the crystal structure of α-NiS, a two-sublattice model (Ni, Va)$_1$(S)$_1$ is simpler and is adequate to reflect the atomic arrangement. As shown in the phase diagram (Fig. 3a), the homogeneity range of α-NiS agrees well with the experimentally determined phase boundary [80,81,117]. In addition, the sulfur vapor pressure is calculated for α-NiS as shown in Fig. 6, where excellent agreement can be found with the experimental work of Lin et al. [102] and Rau [79].

The space group of Ni_9S_8 is C222 (#21) [118]. Ni_9S_8 is reported to

Table 2
Standard enthalpy of formation and standard entropy for different nickel sulfides at 295.15 K. (*recommended value by literature, **calculated from CALPHAD model).

Compound	$\Delta_f H_{298.15}$ (KJ/mol)	$\Delta_f S_{298.15}$ (J/(K.mol))	Ref.	Compound	$\Delta_f H_{298.15}$ (KJ/mol)	$\Delta_f S_{298.15}$ (J/(K.mol))	Ref.
Ni_3S_2		133.89 ± 0.84	[114]	β-NiS		52.97 ± 0.335	[114]
	−215.90 ± 12.52	133.93 ± 2.51	[127]		−94.14 ± 4.18	52.97 ± 0.837	[127]
	−216.3 ± 5.0	133.89 ± 0.4	[43]*		−87.86 ± 6.3	53.0 ± 0.4	[43]*
	−217.2 ± 1.6		[125]		−91.0 ± 1		[125]
	−226.6 ± 2.2		[126]		91.0 ± 3	53 ± 0.4	[128]*
	−214.1	135.48	[18]**		−92.62	54.597	[18]**
	−216.0 ± 8.4	133.8 ± 1.6	[101]		−94.1 ± 4.2	53 ± 0.8	[129]
		133.2	[100]		−91.2	57.0	This work
	−216.3 ± 3.0	133.2 ± 0.3	[128]*	Ni_3S_4	−326.35 ± 25.10	171.3 ± 25.1	[127]
	−217.2 ± 1.6	133.5 ± 0.7	[129]*		−301.1 ± 25.0	186.48 ± 16.7	[43]
	−212.8	132.50	This work*		−309.11	191.89	[18]**
Ni_7S_6	−582.8 ± 5.7		[125]		−318.5	186.8	This work
	−567.11	384.006	[18]**	NiS_2	−133.89 ± 8.4	67.78 ± 8.368	[127]
	−574.05	360.8	This work*		−131.38 ± 16.70	71.97 ± 8.4	[43]
Ni_9S_8	−770.11	468.73	[18]**		−124.9 ± 1.0		[125]
	760 ± 9	481 ± 7	[129]*		−124.01	81.80	[18]**
	−760.2	479.1	This work*		−128.0 ± 7.0	80 ± 8	[129]*
					−134.3	75.9	This work

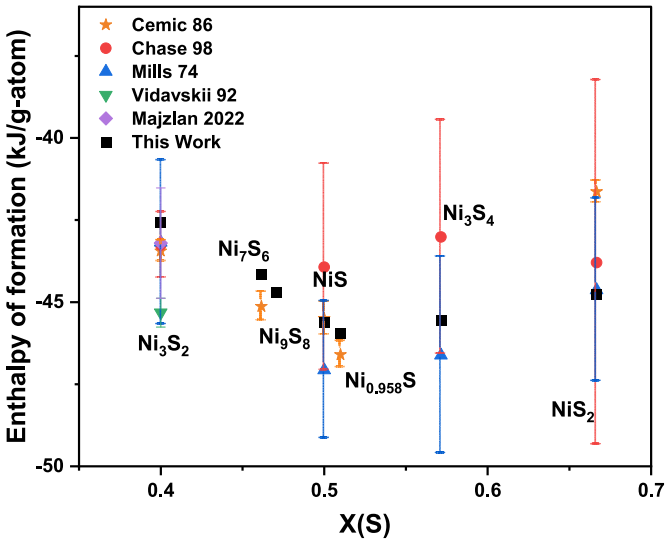

Fig. 7. Calculated enthalpy of formations of the Ni-S binary compounds compared to literature values.

decompose to Ni_7S_6 and α-NiS at 675 K [119]. Accordingly, Ni_7S_6 is stable in the temperature range from 675 K to 846 K. It undergoes a peritectoid reaction at 846 K and forms α-NiS and β_2. It is also found that the Ni_7S_6 phase has a homogeneity range from 45.76 to 46.22 at.% [81]. Stølen et al. have estimated a homogeneity range of 0.56 at.% [119], based on the volume change and crystallographic study reported by Fleet [118]. Considering the narrow homogeneity range, Ni_7S_6 is modeled as a stoichiometric compound, as is suggested by the general practice of dataset development [120]. The heat capacities of Ni_9S_8 and Ni_7S_6 are measured by Stølen et al. [119] from 5 K to 640 K and from 640 K to 900 K, respectively. However, the measured heat capacity of Ni_7S_6 is influenced by the presence of other phases, e.g. α-NiS and β_2, where two endothermic signals were observed at 709K and 797K, respectively. These correspond to the reactions: α-NiS + Ni_7S_6 ⇌ Ni_9S_8 and β_2 ⇌ Ni_7S_6 + Ni_3S_2, respectively. Both endothermic peaks should not be considered for the Gibbs energy description of Ni_7S_6. Therefore, the heat capacity deconvoluted from these two peak are used for the optimization process.

The crystallographic investigation on Ni_3S_4 shows that it has a space group of Fd $\bar{3}$ m (#277) [121]. No experimental information on the heat capacity Ni_3S_4 can be found. A DFT calculation for Ni_3S_4 [122] has

Table 3
Invariant reactions of the Ni-S binary system.

Invariant reaction	x(S) This work			T [K] This work	T [K] Literature	Reference
Liquid ⇌ α-NiS	0			1728.0	1728	[43]
Liquid#1 + Liquid#2 ⇌ NiS_2	0.586	0.984	0.667	1301	1295	[117]
Liquid ⇌ α-NiS	0.519			1264	1272	[117]
Liquid ⇌ α-NiS + NiS_2	0.520	0.534	0.667	1263	1266 ± 3	[117]
Liquid + α-NiS ⇌ β_2	0.437	0.444	0.504	1083	1079	[23]
					1078	[132]
Liquid + β_2 ⇌ β_1	0.425	0.435	0.434	1067	1073	[23,102,130]
Liquid ⇌ (Ni) + β_1	0.330	0	0.367	910.5	910	[130]
β_2 + α-NiS ⇌ Ni_7S_6	0.439	0.500	0.462	842.3	846	[23,81,130]
					848	[132]
β_1 ⇌ Ni_3S_2	0.4			831.0	834	[100,102]
					838	[23]
					838 ± 5	[103]
					823	[132]
					834 ± 1	[131]
β_1 ⇌ Ni_3S_2 + β_2	0.414	0.4	0.421	831.0	~ 833	[100,102]
					837	[23]
					827	[103]
β_1 ⇌ Ni_3S_2 + (Ni)	0.370	0.4	0	812.5	806	[23,130]
β_2 ⇌ Ni_7S_6 + Ni_3S_2	0.430	0.462	0.400	779.8	797	[23,119]
α-NiS + Ni_7S_6 ⇌ Ni_9S_8	0.500	0.462	0.471	711.1	709	[119]
Ni_7S_6 ⇌ Ni_9S_8 + Ni_3S_2	0.462	0.471	0.400	677.8	675	[119]
					673	[132]
α-NiS + Ni_9S_8 ⇌ β-NiS	0.500	0.471	0.500	652.1	660	[111]
					652	[79,102,130]
NiS_2 + α-NiS ⇌ Ni_3S_4	0.667	0.517	0.571	628.8	629	[79,130]
α-NiS ⇌ Ni_3S_4 + β-NiS	0.5	0.571	0.500	555.0	555	[81,130]
Liquid ⇌ NiS_2 + α-S	1	0.667	1	388.4	388.4	[55]
β-S ⇌ α-S	1			368.3	368.3	[55]

Table 4
Thermodynamic parameters of each phase in Ni-S system.

Liquid

$^{0}G_{Ni}^{Liquid} = GOLIQNI + GEIN(207), 1 < T < 3000$

$^{0}G_{NiS}^{Liquid} = GSLIQUID + \mathrm{G0LIQNI} - 4051.736 - 147.859*\mathrm{T}, 1 < T < 3000$

$^{0}G_{S}^{Liquid} = GSLIQUID + GEIN(246.08), 1 < T < 3000$

$^{0}L_{Ni,S}^{Liquid} = 228183.89 + 86.793*T, 1 < T < 3000$

$^{1}L_{Ni,S}^{Liquid} = -65858.66 + 72.92*T, 1 < T < 3000$

$^{2}L_{Ni,S}^{Liquid} = 18243.05, 1 < T < 3000$

$^{4}L_{Ni,S}^{Liquid} = 1760.015, 1 < T < 3000$

$^{0}L_{Ni,NiS}^{Liquid} = -91342.806 + 274.627*T, 1 < \mathrm{T} < 3000$

$^{1}L_{Ni,NiS}^{Liquid} = 53558.486 + -74.157*T, 1 < \mathrm{T} < 3000$

$^{2}L_{Ni,NiS}^{Liquid} = -5380.066, 1 < \mathrm{T} < 3000$

$^{0}L_{Ni,S}^{Liquid} = -45129.262 + -2.432*T, 1 < T < 3000$

FCC-Ni

$^{0}G_{Ni,Va}^{FCC} = G0SERNI + MRNIFCC + GEIN(284) \ 1 < T < 3000$

$^{0}G_{S,Va}^{FCC} = GTORTHS + 80000, 1 < T < 3000$

$^{0}L_{Ni,S}^{FCC} = -24000 + 0.02*T**2, 1 < \mathrm{T} < 3000$

$^{0}G_{S,Va}^{FCC\_A1} = GTORTHS + 80000, 1 < T < 3000$

β_1

$^{0}G_{Ni:S}^{\beta_1} = -124718.134 - .05588*T**2 + GEIN(470.748), 1 < T < 1130$

$^{0}G_{Va:S}^{\beta_1} = 42835.298 + .09791*T^2 + GEIN(26.758), 1 < T < 3000$

$^{0}L_{Ni,Va:S}^{\beta_1} = -133169.565, 1 < T < 3000$

$^{1}L_{Ni,Va:S}^{\beta_1} = 138177.743\ , 1 < T < 3000$

$^{2}L_{Ni,Va:S}^{\beta_1} = -30736.256\ , 1 < T < 3000$

β_2

$^{0}G_{Ni:S}^{\beta_2} = -126936.49 - 0.06805*T^2 + GEIN(753.613), 1 < T < 3000$

$^{0}G_{Va:S}^{\beta_2} = -839.646 + .09546*T^2 + GEIN(30.726), 1 < T < 3000$

$^{0}L_{Ni,Va:S}^{\beta_2} = -62601.235, 1 < T < 3000$

$^{1}L_{Ni,Va:S}^{\beta_2} = 1683.159, 1 < T < 3000$

$^{2}L_{Ni,Va:S}^{\beta_2} = -5380.066, 1 < T < 3000$

α-NiS

$^{0}G_{Ni:S}^{\alpha-NiS} = -102867.990 - 9.040E-03*T^2 - 2.9914E-13*T^5 + 0.9197*GEIN(241.383), 1 < T < 1400$
$= -188642.567 + 573.967*T - 72.818*T*LN(T) + 7.9902E+18*T^{-5} - 3.141E+36*T^{-11}, 1400 < T < 3000$

$^{0}G_{Va:S}^{\alpha-NiS} = 19085.198 - 1.731E-02*T^2 + GEIN(1207.19), 1 < T < 3000$

$^{0}L_{Ni,Va:S}^{\alpha-NiS} = -32424.161, 1 < T < 3000$

$^{1}L_{Ni,Va:S}^{\alpha-NiS} = 5214.520, 1 < T < 3000$

$^{2}L_{Ni,Va:S}^{\alpha-NiS} = -161601.035, 1 < T < 3000$

$^{4}L_{Ni,Va:S}^{\alpha-NiS} = 95159.973, 1 < T < 3000$

Ni_3S_2

$^{0}G_{Ni:S}^{Ni_3S_2} = -257998.670 - 0.011*T^2 - 1.136E-18*T^7 + 0.361*GEIN(175.665) + 0.686*GEIN(460.414), 1 < T < 1080$
$= -407323.354 + 1293.141*T - 166.175*T*LN(T) + 2.0740E+18*T^{-5} + 5.2650E+35*T^{-11}, 1080 < T \langle 6000$

Ni_7S_6

$^{0}G_{Ni:S}^{Ni_7S_6} = -659208.618 - 0.3002*T^2 + 5.369E-05*T^3 + 0.585*GEIN(300.605), 1 < T < 3000$

Ni_9S_8

$^{0}G_{Ni:S}^{Ni_9S_8} = -920993.787 - 2.454E-02*T^2 - 3.917E-29*T^{11} + 0.509*GEIN(170.577) + 0.5754*GEIN(533.960), 1 < T < 750$
$= -1184954.370 + 3053.212*T - 410.546*T*LN(T) - 1.1915E+18*T^{-5} + 7.9510E+34*T^{-11}, 750 < T < 3000$

NiS

$^{0}G_{Ni:S}^{NiS} = -107273.053 - 9.750E-03*T^2 + 5.960E-07*T^3 + 0.768*GEIN(369.325) + 0.159*GEIN(74.834), 1 < T < 3000$

(*continued on next page*)

Table 4 (*continued*)

Ni_3S_4

${}^0G_{Ni:S}^{Ni_3S_4} = -367700.425 - 0.06337*T^2 + 6.554E-10*T^3 + 0.775*GEIN(278.974), 1 < T < 3000$

NiS_2

${}^0G_{Ni:S}^{NiS_2} = -160392.144 - 1.270E-03*T^2 - 1.195E-06*T^3 + 0.5738*GEIN(218.703) + 0.446*GEIN(543.064), 1 < T < 3000$

${}^0Tc_{Ni:S}^{NiS_2} = +31.5;\ {}^0\beta c_{Ni:S}^{NiS_2} = 0.7$

${}^0Tc_{Ni:S}^{NiS_2} = +39;\ {}^0\beta c_{Ni:S}^{NiS_2} = 0.1$

Function *GNILIQ* and *GHSERNI* are cited from Hao et al. [41]

$GTORTHS = -0.00605*T^2 + 4.227E-36*T^5$

$GSLIQUID = -1768.88 - 0.004554*T**2 + G_{polymerization}$

estimated the heat capacity of this compound. However, the calculated result is around 6R at room temperature in this publication with no explanation or comment. Therefore, these data are not used for this optimization. In this regard, the estimated heat capacity values by Chase [43] are used for Ni_3S_4.

NiS_2 is reported to have a space group of Pa $\overline{3}$ (#205). Its heat capacity at low temperature has been reported by Ogawa [123] and Matsuura [124]. It is worth noting that two Néel temperatures at 30.6 K and 39.3 K have been identified in the experiments. This special character is expressed by the Inden-Hillert-Xiong model [28], where both Néel temperatures are defined.

The heat capacities of all the relevant binary phases are summarized in Fig. 4. The calculated results show good agreement to all the selected experimental data.

The measurements of the formation enthalpies for nickel sulfides are carried out by the drop calorimetry measurement from Cemič and Kleppa [125] as well as by direct calorimetric measurement (light pulse induced reaction) by Vidavskii [126]. The formation enthalpies have also been derived from the third-law calculation by Chase [43] and Mills [127]. The calculated formation enthalpies and entropies and the publications are compared with the publications in Table 2 and plotted in Fig. 7, which are in good agreement. The calculated enthalpies for the nickel sulfides are close to a parabola with the only exception being the high-temperature phase α-NiS, as is expected from its the non-stoichiometric nature.

4.4. Superheated temperature range

It should be noted that the Ni_9S_8, α-NiS, and Ni_3S_2 exhibit strong anharmonicity at higher temperatures, which requires high-order terms to describe the heat capacity. Such an exponential increase in the heat capacity is clearly unrealistic and would lead to an erroneous phase diagram at high temperatures, as has been mentioned in the previous sections. There is attempt in this work to extend the method proposed by Rainer Schmidt-Fetzer [39] to the binary intermetallics. However, a strict application of the methodology proposed by the author would lead to a re-stabilization of the binary crystalline phases at higher temperatures. Further protocols are needed as a general approach for the binary intermetallics. In this work, a high-temperature segment is introduced to the Gibbs energy description at the phase transition temperature of the nickel sulfides. This segment ensures continuous and reasonable thermophysical properties of each phase at temperatures well above the melting points. The high temperature β_1 and β_2 are exceptionally stable due to the high heat capacity and high entropy. Such stabilization cannot be addressed with the up-mentioend approach. The High temperature segments of the β_1 and β_2 phase are thus not being modeled.

4.5. Invariant reactions

The invariant reactions of the Ni-S system are evaluated on the basis of the overview by Singleton et al. [130], with some modifications as described below. For the experimental investigation of the Ni-S system on the sulfur rich side, the sulfur evaporation at higher temperatures must be taken into account for an accurate evaluation. The work of Arnold and Malik [117] has revised the previous data of Kullerud and Yund [81], and has included a series of experiments with the correction to the sulfur loss. It is considered a more accurate evaluation for the reactions above 1253 K, including the congruent melting of α-NiS at 1272 ± 3 K, the syntectic reaction: Liquid#1 + Liquid#2 ⇌ NiS_2 at 1295 ± 3 K, and the eutectic reaction: Liquid ⇌ α-NiS + NiS_2 at 1266 ± 3 K.

Ni_3S_2 is reported to transform into the β_1 phase at 833 K by Stølen et al. [100], at 834 K by Ferrante and Gokcen [131], and at 838 K by Kitakaze and Sugaki [22]. The result of Stølen et al. is reliable because of the presentation of detailed DSC measurement data and the consistent results compared to Ferrante and Gokcen [131]. The temperature of the peritectic reaction $\beta_1 \rightleftharpoons Ni_3S_2 + \beta_2$ is estimated to be 833 K by Lin et al. based on the extrapolated phase boundary [102], and 837 K by Kitakaze and Sugaki [22]. The measured phase transition temperature of Kitakaze and Sugaki in this region is too high compared to other authors and is not considered. The high-temperature powder diffraction measurements done by Fjellvåg and Anderson [103] show a phase transition at 827 K at 40.8 at%. The calculated results are tabulated in Table 3, where excellent agreement can be found with the experimental data. The proposed models and parameters for all phases are listed in Table 4.

5. Conclusion

In this work, the thermodynamic description for sulfur has been developed within the framework of the third-generation database approach. Monoclinic sulfur, orthorhombic sulfur as well as liquid sulfur are modeled to fit the experimental data at their stable and metastable temperature ranges. The approach provides a more physically sound extrapolation at temperature range where no experimental data is available. The modeling for the Ni-S binary system is based on the newly developed sulfur dataset and the third-generation database for nickel [14]. The dataset extends the assessment made by Waldner and Pelton [18,19] to 0 K. The superheated solid is described with a polynomial to ensure a continuous and reasonable change of the thermodynamic properties at higher temperatures. All the parameters are treated carefully by taking into account the experimental heat capacity data, phase equilibria, activity data, enthalpy of formation. The sulfur solubility in the FCC nickel is evaluated from the activity measurements in publications. The resultant thermodynamic dataset agrees well with the selected experimental input. The assessment of the metastable state of the phases, especially of the supercooled liquid, will be used for the further thermodynamic investigation of the nickel-sulfur based Pd-Ni-S bulk metallic glass forming liquid.

CRediT authorship contribution statement

Wenhao Ma: Writing – review & editing, Writing – original draft, Software, Methodology, Investigation, Formal analysis. **Julian**

Gebauer: Investigation. **Andreas Klaus Czerny:** Investigation. **Maryam Rahimi Chegeni:** Investigation. **Isabella Gallino:** Writing – review & editing, Supervision, Funding acquisition, Conceptualization. **Ralf Busch:** Writing – review & editing, Supervision, Funding acquisition, Conceptualization. **Hans Jürgen Seifert:** Writing – review & editing, Supervision, Software, Methodology, Funding acquisition, Conceptualization.

Declaration of competing interest

The authors declare the following financial interests/personal relationships which may be considered as potential competing interests: Wenhao Ma reports financial support was provided by German Research Foundation. If there are other authors, they declare that they have no known competing financial interests or personal relationships that could have appeared to influence the work reported in this paper.

Acknowledgement

The authors gratefully acknowledge the funding by the German Research Foundation (project number: 441308809), GA 1721/4-2 and BU 2276/13-2. The authors would like to thank Dr. Peter Franke and Dr. Magnus Rohde for the theoretical support.

Appendix A. Supplementary data

Supplementary data to this article can be found online at https://doi.org/10.1016/j.calphad.2025.102821.

Data availability

Data will be made available on request.

References

[1] M. Queffurus, S.-J. Barnes, A review of sulfur to selenium ratios in magmatic nickel–copper and platinum-group element deposits, Ore Geol. Rev. 69 (2015) 301–324.
[2] K. Zhao, F. Gao, Q. Yang, Comprehensive review on metallurgical upgradation processes of nickel sulfide ores, Journal of Sustainable Metallurgy 8 (2022) 37–50.
[3] J.-H. Wang, M. Liu, Computational study of sulfur–nickel interactions: a new S–Ni phase diagram, Electrochem. Commun. 9 (2007) 2212–2217.
[4] S. Chen, N. Sheng, S. Fan, S. Sun, G. Hou, J. Li, L. Liu, Y. Zhou, X. Sun, Effect of sulfur on microstructures and solidification characteristics of a nickel-base single crystal superalloy, Met. Mater. Int. 28 (2022) 2962–2971.
[5] B. Wong, D. Thomey, L. Brown, M. Roeb, R. Buckingham, C. Sattler, Sulfur Based Thermochemical Energy Storage for Concentrated Solar Power, 2013.
[6] G. Zhou, A. Yang, G. Gao, X. Yu, J. Xu, C. Liu, Y. Ye, A. Pei, Y. Wu, Y. Peng, Y. Li, Z. Liang, K. Liu, L.-W. Wang, Y. Cui, Supercooled liquid sulfur maintained in three-dimensional current collector for high-performance Li-S batteries, Sci. Adv. 6 (2020) eaay5098.
[7] N. Gao, Y. Zhang, C. Chen, B. Li, W. Li, H. Lu, Le Yu, S. Zheng, B. Wang, Low-temperature Li–S battery enabled by CoFe bimetallic catalysts, J. Mater. Chem. A 10 (2022) 8378–8389.
[8] A. Kuball, O. Gross, B. Bochtler, R. Busch, Sulfur-bearing metallic glasses: a new family of bulk glass-forming alloys, Scr. Mater. 146 (2018) 73–76.
[9] A. Kuball, B. Bochtler, O. Gross, V. Pacheco, M. Stolpe, S. Hechler, R. Busch, On the bulk glass formation in the ternary Pd-Ni-S system, Acta Mater. 158 (2018) 13–22.
[10] J. Ågren, Thermodynamics of supercooled liquids and their glass transition, Phys. Chem. Liq. 18 (1988) 123–139.
[11] J. Ågren, B. Cheynet, M.T. Clavaguera-Mora, K. Hack, J. Hertz, F. Sommer, U. Kattner, Workshop on thermodynamic models and data for pure elements and other endmembers of solutions: schloβ ringberg, febr. 21, to march 3, 1995, Calphad 19 (1995) 449–480.
[12] S. Bigdeli, Q. Chen, M. Selleby, A new description of pure C in developing the third generation of calphad databases, J. Phase Equilibria Diffus. 39 (2018) 832–840.
[13] S. Bigdeli, H. Mao, M. Selleby, On the third-generation Calphad databases: an updated description of Mn, physica status solidi (b) 252 (2015) 2199–2208.
[14] L. Hao, A. Ruban, W. Xiong, CALPHAD modeling based on Gibbs energy functions from zero kevin and improved magnetic model: a case study on the Cr–Ni system, Calphad 73 (2021) 102268.
[15] Z. He, B. Kaplan, H. Mao, M. Selleby, The third generation Calphad description of Al–C including revisions of pure Al and C, Calphad 72 (2021) 102250.
[16] A. Walnsch, A. Leineweber, M.J. Kriegel, A third generation CalPhaD assessment of the Fe–Mn–Ti system part I: the binary subsystems Fe–Mn, Fe–Ti and Mn–Ti, Calphad 81 (2023) 102555.
[17] R.C. Sharma, Y.A. Chang, Thermodynamics and phase relationships of transition metal-sulfur systems: IV. Thermodynamic properties of the Ni-S liquid phase and the calculation of the Ni-S phase diagram, Metall. Trans. A B 11 (1980) 139–146.
[18] P. Waldner, A.D. Pelton, Thermodynamic modeling of the Ni–S system, Z. Metallkd. 95 (2004) 672–681.
[19] P. Waldner, Thermodynamic analysis of high-temperature heazlewoodite, Int. J. Mater. Res. 97 (2006) 17–21.
[20] J.M. Larrian, Thermodynamic properties of nickel-sulfur melts, Calphad 3 (1979) 139–157.
[21] F. Kongoli, A.D. Pelton, Y. Dessureault, Thermodynamic modeling of liquid Fe-Ni-Cu-Co-S mattes, Metall. Trans. A B 29 (1998) 591–601.
[22] A. Kitakaze, A. Sugaki, Study of the Ni3+/-xS2 phase in the Ni-S system with emphasis on the phases of high-form Ni3S2 (beta (1)), and Ni4S3 (beta (2)). Neues Jahrbuch fur Mineralogie-Monatshefte, 2001, pp. 41–48.
[23] A. Kitakaze, A. Sugaki, H. Itoh, R. Komatsu, A revision of phase relations in the system Fe-Ni-S from 650 to 450 C, Can. Mineral. 49 (2011) 1687–1710.
[24] H. Okamoto, Ni-S (Nickel-Sulfur), J. Phase Equilibria Diffus. 30 (2009) 123.
[25] I.A. Bajenova, A.S. Ivanov, N.M. Konstantinova, I.A. Uspenskaya, A.V. Khvan, A. T. Dinsdale, A. Kondratiev, A new thermodynamic description of pure silicon from 0 K at 1 bar, Calphad 81 (2023) 102554.
[26] I. Bajenova, A. Khvan, M. Derevyanko, N. Aristova, A. Dinsdale, A. Kondratiev, A. Pisch, Third-generation CALPHAD description of pure GeO2 at 1 atm, Calphad 74 (2021) 102299.
[27] G. Inden, Experimental determination of phase diagrams, in: P.E.A. Turchi, A. Gonis (Eds.), Statics and Dynamics of Alloy Phase Transformations, Springer US, Boston, MA, 1994, pp. 17–43.
[28] W. Xiong, Q. Chen, P.A. Korzhavyi, M. Selleby, An improved magnetic model for thermodynamic modeling, Calphad 39 (2012) 11–20.
[29] E. Gamsjäger, M. Wiessner, Low temperature heat capacities and thermodynamic functions described by Debye–Einstein integrals, Monatshefte für Chemie/ Chemical Monthly 149 (2018) 357–368.
[30] A. Obaied, F. Tang, I. Roslyakova, M. to Baben, "2 1/2th" generation Calphad databases: extrapolating heat capacities of elements and compounds to 0K, Calphad 75 (2021) 102352.
[31] C.A. Becker, J. Ågren, M. Baricco, Q. Chen, S.A. Decterov, U.R. Kattner, J. H. Perepezko, G.R. Pottlacher, M. Selleby, Thermodynamic modelling of liquids: CALPHAD approaches and contributions from statistical physics, Phys. Status Solidi B 251 (2014) 33–52.
[32] M. Palumbo, L. Battezzati, Thermodynamics and kinetics of metallic amorphous phases in the framework of the CALPHAD approach, Calphad 32 (2008) 295–314.
[33] O. Tolochko, J. Ågren, Thermodynamic properties of supercooled Fe-B liquids—a theoretical and experimental study, J. Phase Equil. 21 (2000) 19.
[34] E.D. Alvares, W.J. Botta, J. Ågren, A. Costa e Silva, An assessment of Fe-Nb-B melts using the two-state liquid model, Calphad 68 (2020) 101692.
[35] J.H. Perepezko, J.S. Paik, Thermodynamic properties of undercooled liquid metals, J. Non-Cryst. Solids 61 (1984) 113–118.
[36] W. Kauzmann, The nature of the glassy state and the behavior of liquids at low temperatures, Chem. Rev. 43 (1948) 219–256.
[37] Z. He, F. Haglöf, Q. Chen, A. Blomqvist, M. Selleby, A third generation calphad description of Fe: revisions of fcc, hcp and liquid, J. Phase Equilibria Diffus. 43 (2022) 287–303.
[38] B. Sundman, U.R. Kattner, M. Hillert, M. Selleby, J. Ågren, S. Bigdeli, Q. Chen, A. Dinsdale, B. Hallstedt, A. Khvan, H. Mao, R. Otis, A method for handling the extrapolation of solid crystalline phases to temperatures far above their melting point, Calphad 68 (2020) 101737.
[39] R. Schmid-Fetzer, Third generation of unary calphad descriptions and the avoidance of Re-stabilized solid phases and unexpected large heat capacity, J. Phase Equilibria Diffus. 43 (2022) 304–316.
[40] S. Bigdeli, L.-F. Zhu, A. Glensk, B. Grabowski, B. Lindahl, T. Hickel, M. Selleby, An insight into using DFT data for Calphad modeling of solid phases in the third generation of Calphad databases, a case study for Al, Calphad 65 (2019) 79–85.
[41] L. Hao, C. Shen, N.M. Fortunato, H. Zhang, W. Xiong, Third generation Calphad: thermodynamic assessment of the Ni-Ga system with physics-based models, Calphad 88 (2025) 102797.
[42] B. Meyer, Elemental sulfur, Chem. Rev. 76 (1976) 367–388.
[43] M.W. Chase. NIST-JANAF Thermochemical Tables, 4th Edition, American Institute of Physics, Washington, DC, 1998.
[44] Gmelin's Handbuch der anorganischen Chemie, System 9: Schwefel. Parts A2 and B1. 8. Aufl, Verlag Chemie, Weinheim, 1953.
[45] B.E. Warren, J.T. Burwell, The structure of rhombic sulphur, J. Chem. Phys. 3 (1935) 6–8.
[46] S.C. Abrahams, The crystal and molecular structure of orthorhombic sulfur, Acta Crystallogr. 8 (1955) 661–671.
[47] V. Regnault, Untersuchung über die specifische Wärme einfacher und zusammengesetzter Körper, Ann. Phys. 127 (1840) 213–244.
[48] V. Regnault, Untersuchungen über die specifischen Wärmen, Ann. Phys. 138 (1844) 50–80.
[49] W. Nernst, Der energieinhalt fester stoffe, Ann. Phys. 341 (1911) 395–439.
[50] R. Bunsen, Calorimetrische untersuchungen, Ann. Phys. 217 (1870) 1–31.
[51] P. Mondain-Monval, Calorimetric Research on sulfur and selenium, Bull. Soc. Chim. France 4 (1926) 1349.

[52] A. Wigand, Über spezifische Wärme und spezifisches Gewicht der allotropen Modifikationen fester Elemente, Ann. Phys. 327 (1907) 64–98.
[53] E.D. Eastman, W.C. McGavock, The heat capacity and entropy of rhombic and monoclinic sulfur, J. Am. Chem. Soc. 59 (1937) 145–151.
[54] E.D. West, The heat capacity of sulfur from 25 to 450°, the heats and temperatures of transition and Fusion1,2, J. Am. Chem. Soc. 81 (1959) 29–37.
[55] R.L. Montgomery, The Low Temperature Heat Capacity of Sulfur, 1976.
[56] A.K. Mal'tsev, A.F. Demidenko, Application of the control scheme adiabatic conditions for measuring the low-temperature heat capacity of sulfur (translated), A. F. Tr. Mosk, Khim.-Tekhnol. Inst. 51 (1967) 136–139.
[57] B.S. Hemingway, Heat Capacity and Thermodynamic Properties of Equilibrium Sulfur to the Temperature 388.36 K, and the Heat Capacity of Calorimetry Conference Copper, 1999.
[58] S. Susman, S. Clark Rowland, K.J. Volin, The purification of elemental sulfur, J. Mater. Res. 7 (1992) 1526–1533.
[59] G.A. Berezovskii, I.E. Paukov, Heat-capacity and thermodynamic functions of rhombic sulfur, Zh. Fiz. Khim. 52 (1978) 2677–2679.
[60] G.A. Saunders, Y.K. Yoğurtçu, J.E. Macdonald, G.S. Pawley, R.A. Cowley, The elastic behaviour of orthorhombic sulphur under pressure, Proceedings of the Royal Society of London. A. Mathematical and Physical Sciences 407 (1986) 325–342.
[61] K.A. Gschneidner, Physical properties and interrelationships of metallic and semimetallic elements, Solid State Phys. 16 (1964) 275–426.
[62] Q. Chen, B. Sundman, Calculation of debye temperature for crystalline structures—a case study on Ti, Zr, and Hf, Acta Mater. 49 (2001) 947–961.
[63] R.S. Bradley, The specific heat and other thermodynamic functions of rhombic and monoclinic sulphur and their application to the kinetics and thermodynamics of phase transformation, Trans. Faraday Soc. 50 (1954) 1182–1187.
[64] F. Seitz, The Modern Theory of Solids, McGraw-Hill, 1955.
[65] A.T. Dinsdale, SGTE data for pure elements, Calphad 15 (1991) 317–425.
[66] L.V. Gurvich, I. Veyts, Thermodynamic Properties of Individual Substances: Elements and Compounds, CRC press, 1990.
[67] J.T. Burwell, The unit cell and space group of monoclinic sulphur, Z. Kristallogr. 97 (1937) 123–124.
[68] R.L. Montgomery, Monoclinic sulfur: heat capacity anomaly at 198°K caused by disordering of the crystal structure, Science 184 (1974) 562–563.
[69] R. Steudel, B. Eckert, Solid sulfur AllotropesSulfur allotropes, in: R. Steudel (Ed.), Elemental Sulfur and Sulfur-Rich Compounds I, Springer Berlin Heidelberg, Berlin, Heidelberg, 2003, pp. 1–80.
[70] M. Thackray, Melting point intervals of sulfur allotropes, J. Chem. Eng. Data 15 (1970) 495–497.
[71] H. Braune, O. Möller, Die spezifische Wärme des flüssigen Schwefels, Z. Naturforsch. 9 (1954) 210–217.
[72] T. Yoshioka, The specific heat of liquid sulfur, The science reports of the Tohoku University 44 (1960) 135.
[73] A.V. Tobolsky, Polymeric sulfur and related polymers, J. polym. sci., C Polym. symp. 12 (1966) 71–78.
[74] F. Fehér, G.P. Görler, H.D. Lutz, Beiträge zur Chemie des Schwefels. 108. Schmelzwärme und spezifische Wärme des flüssigen Schwefels. Einfluß von Verunreinigungen, Z. Anorg. Allg. Chem. 382 (1971) 135–148.
[75] K.L. Komarek, E. Miller, G. Schick, Ein Kalorimeter mit konstantem Temperaturgradienten zur Messung spezifischer Wärmen von Flüssigkeiten, Monatsh. Chem. 104 (1973) 1139–1153.
[76] M. Kuballa, G.M. Schneider, Differential thermal analysis under high pressure I: investigation of the polymerisation of liquid sulfur, Ber. Bunsen Ges. Phys. Chem. 75 (1971) 513–516.
[77] S.M.C. Verryn, R.K.W. Merkle, Compositional variation of cooperite, braggite, and vysotskite from the Bushveld Complex, Mineral. Mag. 58 (1994) 223–234.
[78] F. Sommer, Association model for the description of thermodynamic functions of liquid alloys, Int. J. Mater. Res. 73 (1982) 77–86.
[79] H. Rau, Range of homogeneity and defect interaction in high temperature nickel sulfide Ni1−xs, J. Phys. Chem. Solid. 36 (1975) 1199–1204.
[80] H. Rau, Homogeneity range of high temperature Ni3±x S2, J. Phys. Chem. Solid. 37 (1976) 929–930.
[81] G. Kullerud, R.A. Yund, The Ni-S system and related minerals, J. Petrol. 3 (1962) 126–175.
[82] G.A. Meyer, J.S. Warner, Y.K. Rao, H.H. Kellogg, Thermodynamic properties of molten sulfides: Part I. The system Ni−S, Metall. Trans. A B 6 (1975) 229–235.
[83] M. Nagamori, T.R. Ingraham, Thermodynamic properties of Ni-S melts between 700°C and 1100°C, Metall. Trans. A 1 (1970) 1821–1825.
[84] Y.Y. Chuang, The Thermodynamics and Phase Relationships of the Cu-Ni-Fe-S Quaternary System and its Subsystems, Ph.D. Thesis, University of Wisconsin-Madison, WI, 1983.
[85] K. Bornemann, Das system nickel-schwefel, Metallurgie 7 (1910) 667–674.
[86] M. Nagamori, T.R. Ingraham, Thermodynamic properties OF NI-S melts between 700 degrees and 1100 degrees C, Metall. Trans. A 1 (1970), 1821-&.
[87] T. Rosenqivst, A thermodynamic study of the iron, cobalt, and nickel sulfides, Journal of the iron and steel institute 176 (1954) 37–57.
[88] A. Egami, T. Nagakawa, T. Oishi, K. Ono, J. Moriyama, A thermodynamic study of the systems Ni–S and Co–S by CaF2 solid electrolyte galvanic cell technique, Transactions of the Japan institute of metals 27 (1986) 890–897.
[89] C.B. Alcock, L.L. Cheng, A thermodynamic study of dilute solutions of sulphur in liquid iron, cobalt, and nickel, and binary alloys between these metals, Journal of the iron and steel institute 195 (1960) 169–173.
[90] M. Takewaki, T. Azakami, M. Kameda, Activity Measurements of Liquid Nickel-Sulfur System between 800° and 1,200°C, Bulletin of the Research Institute of Mineral Dressing and Metallurgy, vol. 28, Tohoku University, 1972, 113-112.
[91] V.Y. Dashevskii, A.Y. Polyakov, Thermodynamic activity of sulphur in nickel-base melts, Russ. Metall. (1966) 13.
[92] N.F. Fiore, Mid-range ductility minimum in Ni-base superalloys, Reviews on High-Temperature Materials 2 (1975) 373–408.
[93] P.D. Merica, R.G. Waltenberg, Malleability and Metallography of Nickel, US Government Printing Office, 1925.
[94] R.J. Brigham, H. Neumayer, J.S. Kirkaldy, Solubility limit for sulphur in nickel between 637° and 1400° C, Can. Metall. Q. 9 (1970) 525–529.
[95] N. Barbouth, J. Oudar, Solubility and diffusion of sulfur in pure metals and alloys, Mem. Etudes Sci. Rev. Metall. 86 (1989) 777–788.
[96] N. Barbouth, Y. Berthier, M. Assefi, Etude thermodynamique de la solubilite et de la diffusion du soufre dans le palladium, Journal of the Less Common Metals 142 (1988) 269–280.
[97] R.A. Mulford, Grain boundary segregation in Ni and binary Ni alloys doped with sulfur, Metall. Trans. A 14 (1983) 865–870.
[98] D. Kandaskalov, D. Monceau, C. Mijoule, D. Connétable, First-principles study of sulfur multi-absorption in nickel and its segregation to the Ni(100) and Ni(111) surfaces, Surf. Sci. 617 (2013) 15–21.
[99] A. Westgren, Die Kristallstruktur von Ni3S2, Z. Anorg. Allg. Chem. 239 (1938) 82–84.
[100] S. Stølen, F. Grønvold, E.F. Westrum Jr., G.R. Kolonin, Heat capacity and thermodynamic properties of synthetic heazlewoodite, Ni3S2, and of the high-temperature phase Ni3±xS2, J. Chem. Therm. 23 (1991) 77–93.
[101] J. Majzlan, S. Kiefer, K. Lilova, T. Subramani, A. Navrotsky, M. Tuhý, A. Vymazalová, D.A. Chareev, E. Dachs, A. Benisek, Calorimetric study of skutterudite (CoAs2.92) and heazlewoodite (Ni3S2), Am. Mineral. 107 (2022) 2219–2225.
[102] R.Y. Lin, D.C. Hu, Y.A. Chang, Thermodynamics and phase relationships of transition metal-sulfur systems: II. The nickel-sulfur system, Metall. Trans. A B 9 (1978) 531–538.
[103] H. Fjellvåg, A. Andersen, Properties of Ni~ 3S~ 2 at high temperatures, Acta Chem. Scand. 48 (1994) 290.
[104] Z.N. Fedorova, E.F. Sinyakova, Experimental investigation of physicochemical conditions of pentlandite formation, Russian Journal of Geology and Geophysics 34 (1993) 79–87.
[105] S. Karup-Moller, E. Makovicky, The system Pd-Ni-S at 900 degrees 725 degrees 550 degrees and 400 degrees C, Econ. Geol. 88 (1993) 1261–1268.
[106] V.I. Kosyakov, E.F. Sinyakova, V.A. Shestakov, Dependence of sulfur fugacity on the composition of phase associations in the Fe-FeS-NiS-Ni system at 873 K, Geochem. Int. 7 (2003) 660.
[107] H. Yagi, J.B. Wagner, Chemical diffusion and electrical conductivity of Ni 3+-x S 2, Oxid. Metals 18 (1982) 41–54.
[108] G. Liné, M. Huber, Chimie minerale - etude radiocristallographique a haute temperature de la phase non staechiometrique ni3+/-s2, Comptes rendus hebdomadaires des séances de l'Académie des sciences 256 (1963) 3118.
[109] A. Stokłosa, J. Stringer, Defect structure and chemical diffusion in nickel sulfide β-Ni 3 S 2, Oxid. Metals 11 (1977) 277–288.
[110] M. Arita, Thermodynamics of the solid Ni-S system, Metall. Mater. Trans. 37 (2006) 3009–3022.
[111] F. Grønvold, S. Stølen, Heat capacity and thermodynamic properties of millerite from 298.15 to 660 K and NiAs-type nickel (II) sulfide from 260 to 1000 K. Thermodynamics of the NiAs-type to millerite transition, Thermochim. Acta 266 (1995) 213–229.
[112] J.M.D. Coey, R. Brusetti, Heat capacity of nickel sulfide and its semimetal-metal transition, Phys. Rev. B 11 (1975) 671–677.
[113] J. Trahan, R.G. Goodrich, Heat capacity of hexagonal NiS: metal-nonmetal transition, Phys. Rev. B 6 (1972) 199–203.
[114] W.W. Weller, K.K. Kelley, Low-temperature Heat Capacities and Entropies at 298.150 of Sulfides of Arsenic, Germanium and Nickel, US Department of the Interior, Bureau of Mines, 1964.
[115] M. Laffitte, Etude cristallochimique du monosulfure de nickel, Bull. Soc. Chim. Fr. (1959) 1211–1222.
[116] I. Jandl, H. Ipser, K.W. Richter, Thermodynamic modelling of the general NiAs-type structure: a study of first principle energies of formation for binary Ni-containing B8 compounds, Calphad 50 (2015) 174–181.
[117] R.G. Arnold, O.P. Malik, The NiS-S system above 980 degrees C; a revision, Econ. Geol. 70 (1975) 176–182.
[118] M.E. Fleet, Structure of godlevskite, Ni9S8, Acta Crystallogr. Sect. C Cryst. Struct. Commun. 43 (1987) 2255–2257.
[119] S. Stølen, H. Fjellvåg, F. Grønvold, H. Seim, E.F. Westrum Jr., Phase stability and structural properties of Ni7±δS6 and Ni9S8 Heat capacity and thermodynamic properties of Ni7S6 at temperatures from 5 K to 970 K and of Ni9S8 from 5 K to 673 K, J. Chem. Therm. 26 (1994) 987–1000.
[120] R. Schmid-Fetzer, D. Andersson, P.Y. Chevalier, L. Eleno, O. Fabrichnaya, U. R. Kattner, B. Sundman, C. Wang, A. Watson, L. Zabdyr, M. Zinkevich, Assessment techniques, database design and software facilities for thermodynamics and diffusion, Calphad 31 (2007) 38–52.
[121] D. Lundqvist, X-ray studies on the binary system Ni-S, Arkiv foer Kemi, Mineralogi och Geologi 24 (1947) 1–12.
[122] H. Tian, S. Liu, Q. Zhang, Y. Zhao, S. Tan, Y. Li, First-principles calculations of thermodynamic properties of Ni sulfides in the upper mantle, Phys. Chem. Miner. 48 (2021) 30.

[123] S. Ogawa, Specific heat study of magnetic ordering and band structure of 3d transition metal disulfides having the pyrite structure, J. Phys. Soc. Jpn. 41 (1976) 462–469.
[124] M. Matsuura, Y. Endoh, H. Hiraka, K. Yamada, A.S. Mishchenko, N. Nagaosa, I. V. Solovyev, Classical and quantum spin dynamics in the fcc antiferromagnet NiS2 with frustration, Phys. Rev. B 68 (2003) 94409.
[125] L. Cemić, O.J. Kleppa, High temperature calorimetry of sulfide systems. I. Thermochemistry of liquid and solid phases of Ni + S, Geochem. Cosmochim. Acta 50 (1986) 1633–1641.
[126] L.M. Vidavskii, I.I. Korotkevich, The standard molar enthalpy of formation of heazlewoodite Ni3S2 determined by its synthesis in a calorimeter, J. Chem. Therm. 24 (1992) 577–584.
[127] K.C. Mills, Thermodynamic Data for Inorganic Sulphides, Selenides and Tellurides, 1974.
[128] R.A. Robie, B.S. Hemingway, Thermodynamic Properties of Minerals and Related Substances at 298.15 K and 1 Bar (10^5 Pascals) Pressure and at Higher Temperatures, 1995.
[129] H. Gamsjäger, J. Bugajski, W. Preis, Chemical Thermodynamics of Nickel, Elsevier, Amsterdam, 2005.
[130] M. Singleton, P. Nash, K.J. Lee, Ni-S (Nickel-Sulfur), ASM International, 1991.
[131] M.J. Ferrante, N.A. Gokcen, Relative Enthalpies of Ni3S2, US Department of the Interior, Bureau of Mines, 1982.
[132] M.A. Sokolova, Investigation of the system Ni-S (from 30, 0 to 50, 0 at. percent S), Zh. Neorg. Khim. 1 (1956) 1440–1454.